© 2022. Published by The Company of Biologists Ltd | Development (2022) 149, dev200286. doi:10.1242/dev.200286

RESEARCH REPORT

Hemocytes are essential for *Drosophila melanogaster* post-embryonic development, independent of control of the microbiota

Holly N. Stephenson[1,2,*], Robert Streeck[1,*], Florian Grüblinger[1], Christian Goosmann[1] and Alf Herzig[1,‡]

ABSTRACT

Proven roles for hemocytes (blood cells) have expanded beyond the control of infections in *Drosophila*. Despite this, the crucial role of hemocytes in post-embryonic development has long thought to be limited to control of microorganisms during metamorphosis. This has previously been shown by rescue of adult development in hemocyte-ablation models under germ-free conditions. Here, we show that hemocytes have an essential role in post-embryonic development beyond their ability to control the microbiota. Using a newly generated strong hemocyte-specific driver line for the GAL4/UAS system, we show that specific ablation of hemocytes is early pupal lethal, even under axenic conditions. Genetic rescue experiments prove that this is a hemocyte-specific phenomenon. RNA-seq data suggests that dysregulation of the midgut is a prominent consequence of hemocyte ablation in larval stages, resulting in reduced gut lengths. Dissection suggests that multiple processes may be affected during metamorphosis. We believe this previously unreported role for hemocytes during metamorphosis is a major finding for the field.

KEY WORDS: *Drosophila*, Hemocytes, Metamorphosis, Pupal lethal

INTRODUCTION

Drosophila melanogaster is an important model to study both the immune and non-immune related functions of blood cells (hemocytes) (Mase et al., 2021). Plasmatocytes are macrophage-like cells (~95% of larval hemocytes) that secrete signaling peptides, anti-microbial peptides, and extracellular matrix (ECM) proteins in addition to phagocytosing microorganisms and apoptotic cells (Olofsson and Page, 2005; Braun et al., 1998). Crystal cells (~5% of larval hemocytes) express high levels of pro-phenoloxidases, which catalyze the extracellular production of melanin and toxic by-products upon cell lysis; essential for wound closure and immunity (Binggeli et al., 2014). Lamellocytes, rarely found in healthy larvae, transdifferentiate in large numbers from plasmatocytes to encapsulate large pathogens (Sinenko et al., 2011). Recent single-cell RNA-seq studies have shown greater heterogeneity in these cell types (Cattenoz et al., 2020; Tattikota et al., 2020; Coates et al., 2021).

Two waves of hematopoiesis occur in *Drosophila* development. Embryonic hemocytes originate from the head mesoderm; they are long-lived, many surviving into the adult stage (Tepass et al., 1994). Larval hematopoiesis occurs in the lymph gland and in hematopoietic pockets (HP), patches of sessile hemocytes associated with the larval cuticle. HP are the main source of increasing numbers of circulating hemocytes during larval development (Leitao and Sucena, 2015); whereas hemocytes from the lymph gland are released into circulation at early metamorphosis (Jung et al., 2005).

Genetic ablation studies that aimed to identify the importance of hemocytes in *Drosophila* were first performed over a decade ago (Charroux and Royet, 2009; Nehme et al., 2011; Defaye et al., 2009; Shia et al., 2009; Arefin et al., 2015). A 60-75% reduction in larval hemocyte numbers was achieved by hemocyte-specific expression of pro-apoptotic transgenes, ablating cells through programmed cell death. Multiple studies showed a reduction in eclosion of adult flies of up to 60%; interestingly however, eclosion rates were rescued when larvae were reared with antibiotics or under germ-free (GF) conditions (Arefin et al., 2015; Charroux and Royet, 2009; Defaye et al., 2009; Shia et al., 2009). This suggested control of microorganisms by hemocytes is crucial during metamorphosis, and that hemocyte functions beyond immunity are non-essential for post-embryonic development (Charroux and Royet, 2009; Shia et al., 2009; Arefin et al., 2015; Defaye et al., 2009). In contrast, ablation of embryonic hemocytes is embryonic lethal, independent of control of microorganisms (Defaye et al., 2009; Shia et al., 2009).

In this study, we designed an improved *Drosophila* hemocyte-specific larval and adult driver line, Hml^{P2A}-GAL4. Using Hml^{P2A}-GAL4-driven apoptosis, we almost completely ablated hemocytes in the larvae. We show for the first time that hemocytes are essential for the development of adult stage flies, independent of control of the microbiota. RNA-seq data show a striking upregulation of genes in the midgut of 'hemoless' larvae, and points to a crucial role of hemocytes in regulating intestinal development and beyond.

RESULTS AND DISCUSSION

Hml^{P2A}-GAL4 is a hemocyte-specific driver

Currently, the most widely used hemocyte-specific driver in larvae and adults is Hml^{Δ}-GAL4, which uses 840 bp of the *Hml* enhancer (Sinenko and Mathey-Prevot, 2004). To generate an optimized enhancer element, we included the first nine exons of *Hml* followed by a P2A self-cleaving sequence upstream of GAL4 (Hml^{P2A}-GAL4) (Fig. S1). Transgenic flies were generated at two landing-sites, attP40 and attP2.

[1]Department of Cellular Microbiology, Max Planck Institute for Infection Biology, Charitéplatz 1, Berlin 10117, Germany. [2]Peninsula Medical School, Faculty of Health, University of Plymouth, Plymouth, Devon PL4 8AA, UK.
*These authors contributed equally to this work

‡Author for correspondence (herzig@mpiib-berlin.mpg.de)

A.H., 0000-0003-4246-4666

Handling Editor: Paul Martin
Received 21 October 2021; Accepted 19 August 2022

Development (2022) 149, dev200286. doi:10.1242/dev.200286

To analyze expression, we combined *Hml*^{P2A}-GAL4 driving expression of EGFP (*Hml*^{P2A}>GFP) with *srp*^{Hemo}-QF2 driving mCherry (*srp*^{Hemo}>mCherry) (Fig. 1; Fig. S2). *srp*^{Hemo}-QF2 derives from the *serpent* enhancer and drives expression in embryonic and larval hemocytes (Gyoergy et al., 2018) as well as pericardial nephrocytes and Garland cells (Das et al., 2008). Consistent with the reported onset of *Hml* expression during first larval instar (Defaye et al., 2009), *srp*^{Hemo}-positive (*srp*^{Hemo}+) hemocytes in stage 17 embryos were mostly *Hml*^{P2A}-negative (*Hml*^{P2A}−), although faint expression was detected in some cells (Fig. S2B). In late first larval instar (Fig. 1A-C) *Hml*^{P2A} expression overlapped with *srp*^{Hemo} expression in peripheral HP with some hemocytes still *Hml*^{P2A}− (Fig. 1B), and independent of *srp*^{Hemo} in the developing lymph gland (Fig. 1C). In late third larval instar wandering stage (WS) (Fig. 1D-F), *Hml*^{P2A}+ hemocytes were a mixture of *srp*^{Hemo}− and *srp*^{Hemo}+ (Fig. 1E); lymph gland *Hml*^{P2A}+ hemocytes were all *srp*^{Hemo}− (Fig. 1F). This correlates with previous reports that *srp*^{Hemo} is expressed in hemocytes solely deriving from embryonic hematopoiesis (Bruckner et al., 2004). Overlap between *Hml*^{P2A} and *srp*^{Hemo} was restricted to hemocytes during the entire development and we did not observe *Hml*^{P2A} expression outside hemocytes (Fig. S2).

We next used hemocyte-specific antibodies to determine the coverage of *Hml*^{P2A} expression in hemocytes (Fig. 1G-L). The overlap between *Hml*^{P2A} expression and the plasmatocyte marker Nimrod C1 (Kurucz et al., 2007a) was >80% (Fig. 1G,H). Overlap with the pan-hemocyte marker Hemese (Kurucz et al., 2003) was ∼98% (Fig. 1I,J). Similar to the *in vivo* data, all *srp*^{Hemo}+ hemocytes

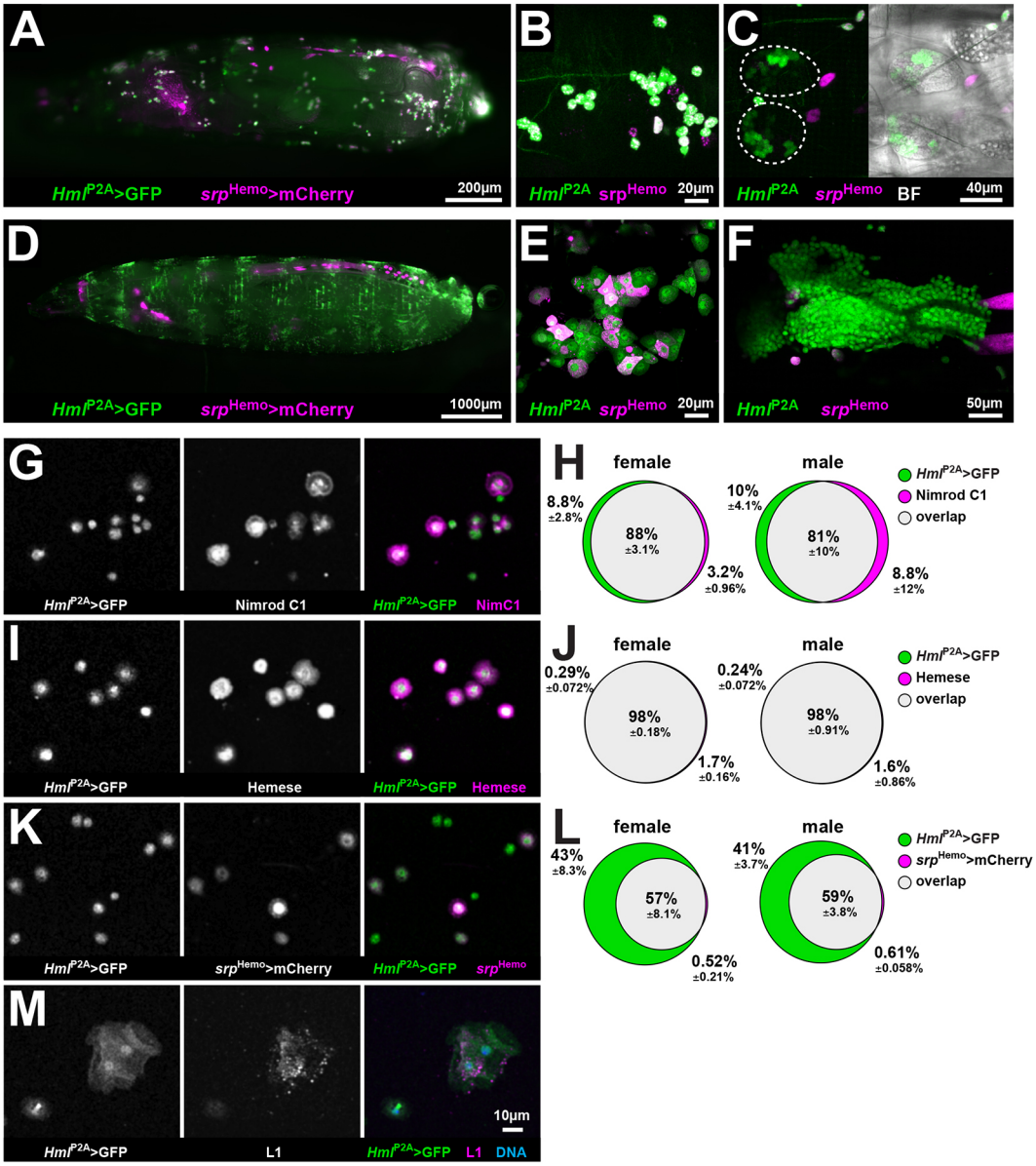

Fig. 1. *Hml*^{P2A}-GAL4 is a hemocyte-specific driver. (A-F) Fluorescent microscopy of *Hml*^{P2A}>GFP (attP40); *srp*^{Hemo}>mCherry first instar (A-C) and WS-larvae (D-F). Whole animals (A,D); maximum projections of image stacks including peripheral hematopoietic pockets (B,E) and developing lymph gland (C,F). BF indicates brightfield images. (G-M) Fluorescent microscopy analysis (G,I,K,M) of hemocytes extracted from *Hml*^{P2A}>GFP (attP40); *srp*^{Hemo}>mCherry WS-larvae stained with plasmatocyte-specific (Nimrod C1), pan-hemocyte (Hemese) or lamellocyte-specific (L1) antibodies. Euler diagrams (H,J,L) show overlap of stainings and *Hml*^{P2A}>GFP expression from $n \geq 3$ independent experiments, >30,000 cells analyzed. Overlap between L1 staining and *Hml*^{P2A}>GFP expression was 95% (s.d. 6.8%) from a total of 211 cells analyzed from five independent experiments.

Development (2022) 149, dev200286. doi:10.1242/dev.200286

were Hml^{P2A}+ in WS-larvae, whereas only ∼60% of Hml^{P2A}+ hemocytes were srp^{Hemo}+ (Fig. 1K,L). Very few lamellocytes were detected using the L1 antibody (Kurucz et al., 2007b) but, of those detected, 95% were Hml^{P2A}+ (Fig. 1M).

Hml^{P2A}-GAL4 is a stronger driver than Hml^{Δ}-GAL4

To compare the expression strength of Hml^{P2A}-GAL4 and Hml^{Δ}-GAL4 we assayed extracted hemocytes from Hml^{P2A}>GFP and Hml^{Δ}>GFP WS-larvae by flow cytometry (Fig. S3A). Hml^{P2A}>GFP (attP2 and attP40) hemocytes showed ∼4-fold higher EGFP expression than Hml^{Δ}>GFP hemocytes, which was consistent with microscopy of WS-larvae and adults (Fig. S3B,C).

To compare the efficiency of hemocyte ablation between Hml^{P2A}-GAL4 and Hml^{Δ}-GAL4, we used them to drive expression of the pro-apoptotic gene *reaper* (*rpr*) or the mouse BCL2-associated X protein gene (*Bax*). Consistent with previous studies (Arefin et al., 2015; Charroux and Royet, 2009; Defaye et al., 2009; Shia et al., 2009), Hml^{Δ}-GAL4 induced significant but incomplete ablation of total blood cells or crystal cells (Fig. 2A,B; Fig. S3D-F). Hml^{P2A}-GAL4 (attP2) improved the efficiency of *rpr*-mediated ablation to >99% in both cases (Fig. 2A,B). We verified ablation of plasmatocytes by staining for Nimrod C1 and Hemese (Fig. 2C). We also identified Hemese-positive lamellocytes by cell morphology, but observed no depletion despite Hml^{P2A} expression in lamellocytes (Fig. 1M). In contrast to previous studies with Hml^{Δ}-GAL4, we neither observed increased lamellocyte numbers, nor melanotic masses in Hml^{P2A}>*rpr* or Hml^{P2A}>*Bax* larvae (n>20) (Arefin et al., 2015; Defaye et al., 2009).

To follow the dynamics of hemocyte ablation *in vivo* we combined Hml^{P2A}>*rpr* with srp^{Hemo}>mCherry. The ablation pattern correlated with expression analysis (Fig. 2D). Few srp^{Hemo}+ hemocytes were still detected by the end of first larval instar [24 h after larval hatching (ALH)], but from late second instar onwards (48 h ALH) we only detected cell remnants. Hemocytes associate with multiple tissues (Cox et al., 2021; Gyoergy et al., 2018; Ayyaz et al., 2015). To address the ablation of tissue-resident hemocytes we dissociated WS-larvae and assessed cells by flow cytometry (Fig. 2E). srp^{Hemo}+ hemocytes comprised ∼5% of live single cells in controls, but were eliminated in Hml^{P2A}>*rpr* larvae. Together, this shows that Hml^{P2A} allows almost complete ablation of plasmatocytes and crystal cells.

Hemocyte ablation with Hml^{P2A}-GAL4 is pupal lethal under germ-free conditions

Previous Hml^{Δ}-GAL4 ablation studies showed a reduction in eclosion rates that were rescued by antibiotic treatment or GF conditions (Arefin et al., 2015; Charroux and Royet, 2009; Defaye et al., 2009; Shia et al., 2009). Given the improved ablation rate of hemocytes using Hml^{P2A}-GAL4, we revisited this observation (Fig. 3; Fig. S4). First, we compared survival rates between Hml^{P2A}-GAL4- and Hml^{Δ}-GAL4-driven hemocyte ablation. Eclosion rates of Hml^{Δ}>*rpr* and Hml^{Δ}>*Bax* pupae were reduced by ∼25%; this reduction was less than previously reported (Arefin et al., 2015; Charroux and Royet, 2009; Defaye et al., 2009; Shia et al., 2009), but still statistically significant (Fig. 3A; Fig. S4B). Strikingly, eclosion rates of Hml^{P2A}>*rpr* and Hml^{P2A}>*Bax* pupae dropped to <5% (Fig. 3A; Fig. S4B). We then reared larvae with antibiotics (5 mg/ml ampicillin, 5 mg/ml kanamycin) or under GF conditions as previously described (Charroux and Royet, 2009; Defaye et al., 2009). Eclosion rates of Hml^{Δ}>*rpr* and Hml^{Δ}>*Bax* pupae were restored to control levels (Fig. 3B; Fig. S4B). In contrast, Hml^{P2A}>*rpr* and Hml^{P2A}>*Bax* pupae did not eclose (Fig. 3B; Fig. S4B). This pointed to an essential role for hemocytes during pupal development, independent of control of the microbiota.

Next, we analyzed lethality in more detail comparing both Hml^{P2A} driver lines (Fig. 3C-E; Fig. S4C,D). Larval survival was not affected under GF and conventional conditions (Fig. 3C; Fig. S4C). Larval development was extended for all genotypes under GF conditions but, relative to controls, pupariation of Hml^{P2A}>*rpr* was only slightly delayed under conventional conditions (Fig. 3C; Fig. S4C). Eclosion rates were ∼10% for Hml^{P2A}>*rpr* (attP40) and <1% for Hml^{P2A}>*rpr* (attP2) (Fig. 3D). The eclosion rate for Hml^{P2A}>*rpr* (attP40) was reduced to ∼2% under conventional conditions (Fig. S4C). To further characterize pupal lethality we scored the end-point of pupal development into three categories (Bainbridge and Bownes, 1981); arrest before pupal stage P8 (light pupae, Fig. 3D,E), between P8-P14 (pharate, Fig. 3D,E) or during P15 (failed eclosion, Fig. 3D). The majority of 'hemoless' pupae died before P8, with no visible eye coloration. For Hml^{P2A}>*rpr* (attP2) this was almost 100% and not affected by GF conditions. For Hml^{P2A}>*rpr* (attP40), GF conditions reduced the fraction of pupae that died during pharate stages (P8-14, Fig. 3D,E) and increased the number of failed eclosions and adults. This suggested that GF conditions primarily affected late pupal development. All surviving adults showed a non-inflated wing phenotype and we found residual hemocytes in escapers from Hml^{P2A}>*rpr; srp*^{Hemo}>mCherry (Fig. S4D). Together, this indicated that Hml^{P2A}>*rpr* (attP2) causes a slightly stronger, more penetrant phenotype, which we further analyzed. Hml^{P2A}>*rpr* (attP2) pupae showed defects during pupariation (non-retracted mouth hooks, non-everted anterior spiracles) and by 24 h post-pupariation 95% of pupae (n=101) had a large posterior gas bubble (Fig. S4E). This likely reflects failure to complete stage P4 (ii), the 'moving bubble' stage (Bainbridge and Bownes, 1981). In summary our data suggests, that 'hemoless' pupae die during early metamorphosis.

Eclosion rates are rescued with hemocyte-specific expression of GAL80

In order to minimize the chance that pupal lethality in our ablation experiments was caused by off-target expression of Hml^{P2A}-GAL4, we performed genetic rescue experiments with hemocyte-specific expression of the GAL4 inhibitor, GAL80. Eclosion rates of Hml^{P2A}>*rpr* (attP2) were rescued by Hml^{Δ}-QF2 driving QUAS-GAL80 (Hml^{Δ}>GAL80), showing that Hml^{P2A}-GAL4 has no crucial off-target expression compared with the original *Hml* driver (Fig. 3F; Fig. S4F). We then used srp^{Hemo}, either directly driving GAL80 (srp^{Hemo}-GAL80) or via srp^{Hemo}-QF2 (srp^{Hemo}>GAL80) to rescue Hml^{P2A}>*rpr* (attP2) or Hml^{P2A}>*rpr* (attP40), respectively (Fig. 3F; Fig. S4F). Based on the observation that srp^{Hemo} and Hml^{P2A} expression exclusively overlap in hemocytes (Fig. 1), this indicates that Hml^{P2A}>*rpr* lethality is caused by hemocyte ablation.

Hemocyte ablation leads to dysregulation of midgut-expressed genes

To analyze the consequences of hemocyte ablation before lethality in early pupal stages, we generated RNA-seq datasets for whole WS-larvae and isolated plasmatocytes and classified transcripts as: (1) not expressed in plasmatocytes, (2) similarly present in both datasets (shared) or (3) enriched in plasmatocytes (Fig. 4A). To address potential systemic responses we further analyzed tissue-specific enrichment of transcripts based on data available at FlyAtlas2 (Leader et al., 2018) (Fig. S5B). Plasmatocyte-enriched transcripts were detected to a variable degree in multiple tissues (Fig. S5B), reflecting either low-level expression outside plasmatocytes or the presence of plasmatocytes in these tissues

Development (2022) 149, dev200286. doi:10.1242/dev.200286

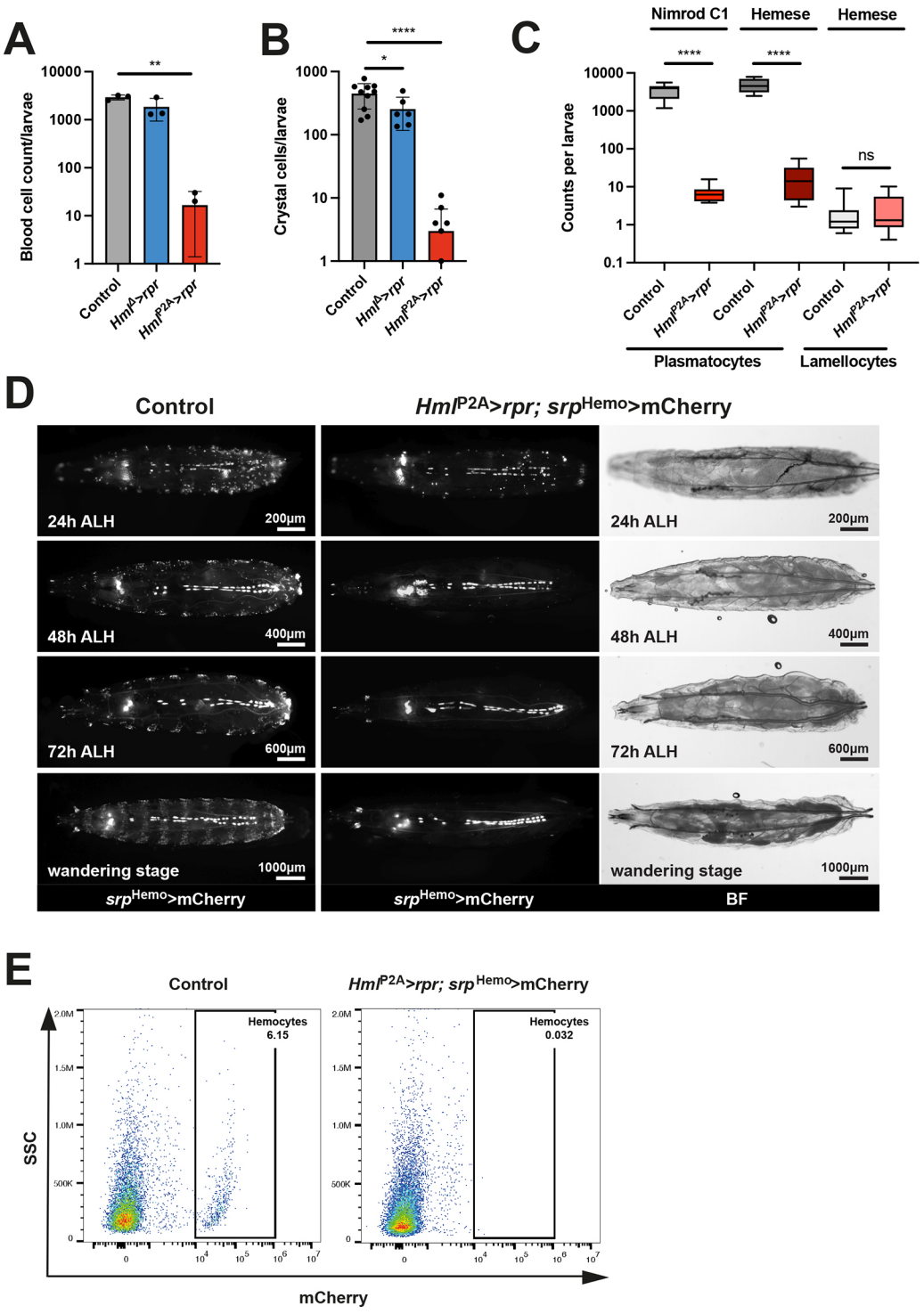

Fig. 2. Inducing apoptosis with *Hml*^{P2A}-GAL4 ablates virtually all plasmatocytes and crystal cells. (A-C) Hemocyte ablation in *Hml*^{P2A}>*rpr* (attP2) WS-larvae. Whole blood cell counts by hemocytometer (A), crystal cell counts by whole mount microscopy (B) and quantification based on staining with plasmatocyte-specific (Nimrod C1) or pan-hemocyte (Hemese) antibodies (C). Hemese-positive lamellocytes were identified by cell morphology. Each dot represents average counts from five animals (A,C) or a single animal (B). One-way ANOVA (A,B) and two-tailed unpaired *t*-tests (C) were performed. Data are mean±s.d. (A,B). Box plots (C) show median values (middle bars) and first to third interquartile ranges (boxes); whiskers indicate minimum and maximum values. (D,E) Hemocyte ablation in *Hml*^{P2A}>*rpr* (attP40); *srp*^{Hemo}>mCherry larvae. (D) Whole-mount fluorescence microscopy of late first (24 h ALH), late second (48 h ALH), mid third (72 h ALH) and WS-larvae. BF indicates brightfield images. (E) Flow cytometry of cells from dissociated WS-larvae. Representative flow cytometry data from three independent experiments showing side scatter (SSC) and mCherry signals. Controls: attP2>*rpr* (A,B), yw>*rpr* (C), *Hml*^{P2A}>GFP (attP40); *srp*^{Hemo}>mCherry (D,E). *P<0.03; **P<0.002; ****P<0.0001. ns, not significant.

(Ayyaz et al., 2015; Cattenoz et al., 2020; Cox et al., 2021). Known hemocyte-specific transcripts (*Hml*, *He*, *eater*, *Pxn* and *NimC1*) were detected as plasmatocyte-enriched (Fig. 4A) and present in the larval carcass (Fig. S5B), likely due to the association of sessile hemocytes with the cuticle or lymph glands in the carcass. These transcripts were also significantly depleted in the differential

Development (2022) 149, dev200286. doi:10.1242/dev.200286

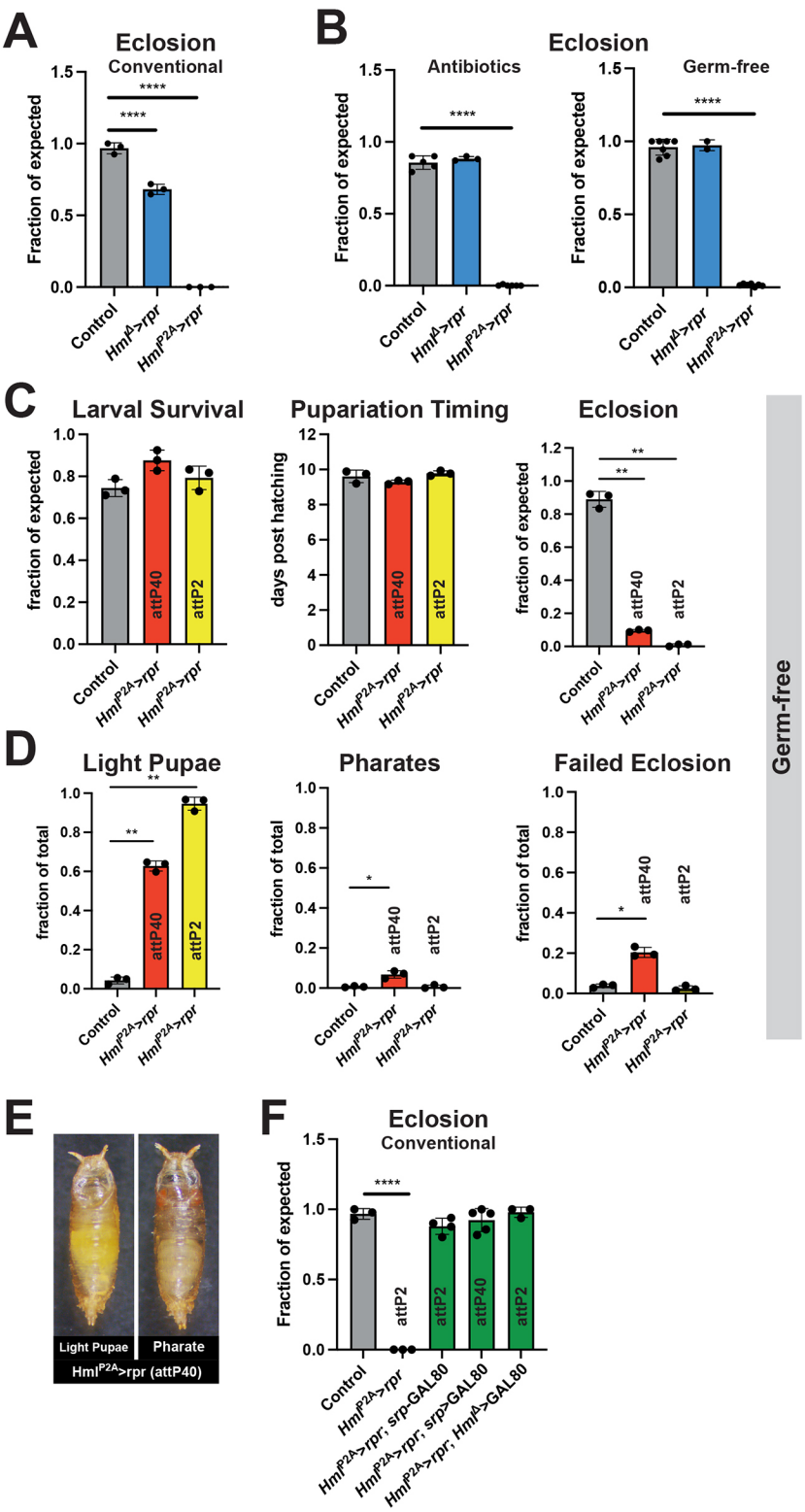

Fig. 3. Hemocyte ablation with *Hml*^{P2A}-GAL4 is pupal lethal under germ-free conditions. (A,B) Eclosion rates of *Hml*$^{\Delta}$>*rpr* and *Hml*^{P2A}>*rpr* (attP2) animals reared at controlled density under conventional conditions (A) or on food containing 5 mg/ml ampicillin and 5 mg/ml kanamycin or under GF conditions (B). Eclosion rates were scored as number of adults obtained from pupae that were formed per vial. Each dot represents an individual vial. One-way ANOVA. (C,D) Comparison of *Hml*^{P2A}-GAL4 driver inserted in attP40 or attP2 based on controlled density cultures raised under GF conditions. (C) Larval survival was scored as pupae obtained from inoculated first instar larvae. Eclosion rates were scored as number of adults obtained from pupae that were formed. Pupariation timing was scored as average over the day of pupariation for each pupae in one vial. (D) Pupal lethality was scored by determining the fraction of all pupae in a vial that terminated development before pupal stage P8 (light pupae), during stage P8-P14 (pharates) or in P15 (failed eclosion). Each dot represents an independent experiment including four vials each (C,D). One-way ANOVA. (E) Representative images of dead pupae from *Hml*^{P2A}>*rpr* (attP40) used to classify light pupae (before pupal stage P8) or pharate adult stage in D. (F) Genetic rescue experiments with controlled density cultures raised under conventional conditions. *Hml*^{P2A}>*rpr* (attP2) was rescued by *srp*^{Hemo}-GAL80, *Hml*^{P2A}>*rpr* (attP40) by *srp*^{Hemo}>GAL80 or *Hml*$^{\Delta}$>GAL80. Eclosion rates were scored as number of adults obtained from pupae formed per vial, each dot represents one vial. One-way ANOVA. Controls: attP2>*rpr* (A,B,F), yw>*rpr* (C,D). Data are mean±s.d. **P*<0.03; ***P*<0.002; *****P*<0.0001.

expression analysis between *Hml*^{P2A}>*rpr* and control larvae (Fig. 4B; Table S1).

We could not identify a tissue-specific response for downregulated transcripts, as only a minority of them were non-plasmatocyte (46/131, Fig. S5C) and Gene Ontology (GO) analysis revealed phagocytosis as the only significantly enriched process or function. In contrast, upregulated transcripts primarily comprised non-plasmatocyte transcripts (131/170) and a majority of them was expressed in the midgut (Fig. 4C; Fig. S5C). GO term analysis showed a strong enrichment of genes associated with chitin metabolism (Fig. 4C). To further analyze phenotypic differences in larval gut morphology, we dissected guts from WS-larvae and analyzed them using electron microscopy (EM) and fluorescent microscopy. Larval gut lengths were significantly decreased in *Hml*^{P2A}>*rpr* compared with control (Fig. 4D; Fig. S6A,B). However, we did not observe a striking difference in gut

Development (2022) 149, dev200286. doi:10.1242/dev.200286

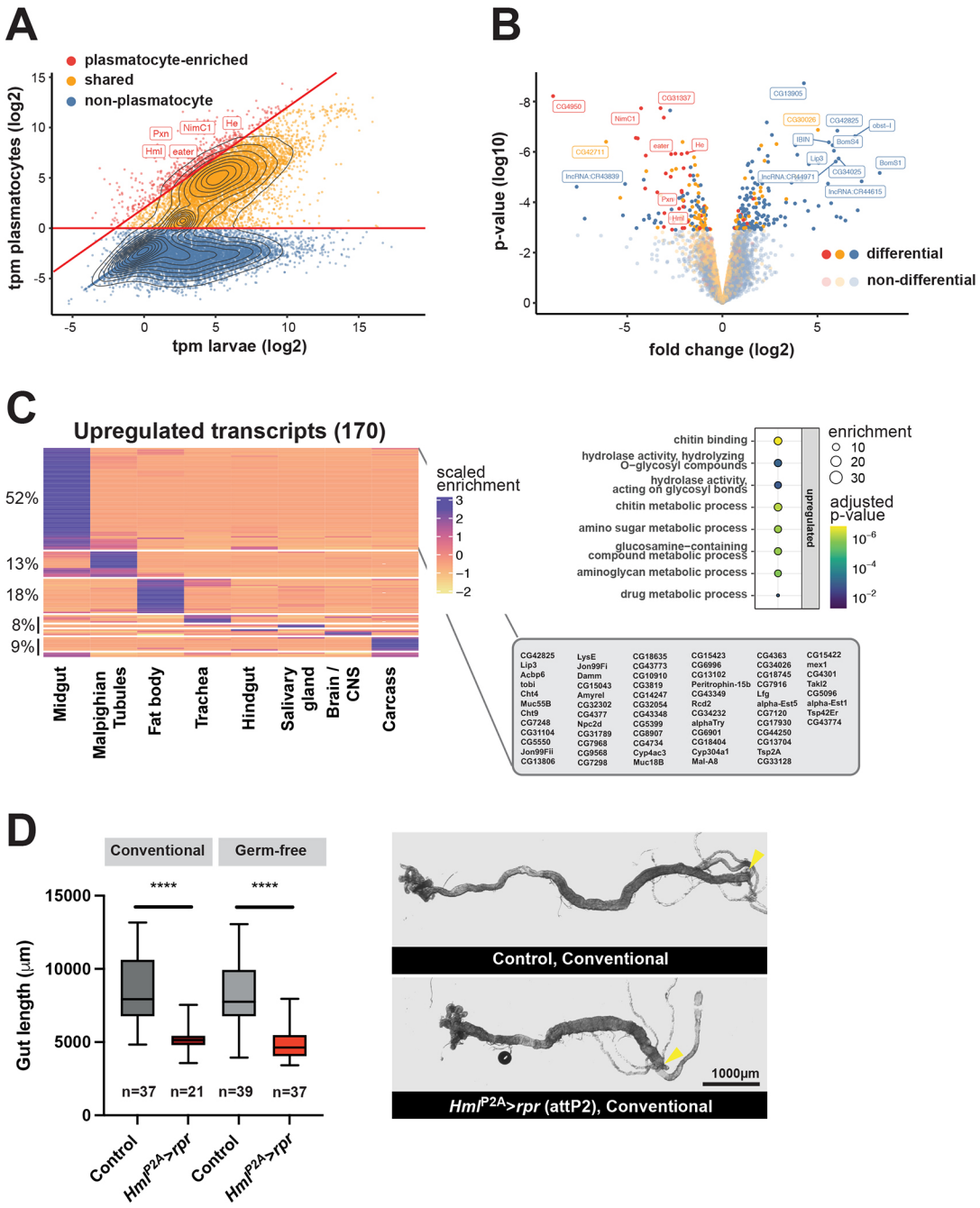

Fig. 4. RNA-seq analysis of 'hemoless' WS-larvae. (A) RNA-seq expression analysis comparing relative expression strength (in tags per million; tpm) of transcripts in whole larvae with expression in larval plasmatocytes (both WS-larvae). Dots represent individual transcripts with overlaid density plot. Genes were classified as non-plasmatocyte (no or marginal expression in plasmatocytes; blue), shared (yellow) or plasmatocyte-enriched (>4 fold elevated in plasmatocytes; red). Hemocyte-specific transcripts are labeled. (B) Volcano plot illustrating differential transcriptome analysis of *Hml*^{P2A}*>rpr* versus *attP2>rpr* WS-larvae. Dots mark log2 fold changes and log10 differential expression *P*-values for individual genes. Genes are colored by assignment as in A, with non-significantly regulated transcripts in lighter colors. The 15 most significantly regulated transcripts and hemocyte-specific transcripts are labeled. (C) Heatmap showing scaled tissue enrichment derived from FlyAtlas2 for upregulated protein coding transcripts. The fraction of transcripts within each k-means cluster is indicated in percent, the tissue type below the heatmap. A list of midgut-specific transcripts that were upregulated in response to hemocyte ablation is shown. Gene ontology terms enriched within upregulated transcripts, *P*-values and enrichment effect sizes are indicated. (D) Midgut lengths from female *Hml*^{P2A}*>rpr* (attP2) versus yw*>rpr* (Control) WS-larvae reared under conventional or GF conditions and dissected in Schneider's media (containing Ca^{2+}). Midgut length was determined from the anterior of whole guts (left) to the attachment site of Malpighian tubules that mark transition to the hindgut (yellow arrowhead). Number of guts are indicated. One-way ANOVA. Box plot shows median values (middle bars) and first to third interquartile ranges (boxes); whiskers indicate minimum and maximum values. ****P<0.0001.

architecture by either EM or fluorescent microscopy (Fig. S6C,D). Dissected *Hml*^{P2A}*>rpr* pupal guts 24 h post-pupariation resembled control guts from 12 h post-pupariation, which is approximately the time point at which *Hml*^{P2A}*>rpr* lethality starts (stage P4, Fig. S6E).

Taken together, we have shown an essential role for hemocytes in post-embryonic development beyond the control of microorganisms. Hemocyte ablation in our model starts in early larval development and appears to be complete by mid-larval stages. The main

Development (2022) 149, dev200286. doi:10.1242/dev.200286

advantages of our model compared with previous systems are improved transgene expression over Hml^{Δ} and higher specificity for hemocytes compared with srp^{Hemo}. In contrast to previous studies, we achieved depletion of hemocytes to <1% of control animals, which leads to pupal lethality that can no longer be rescued by GF conditions. One of these studies showed that hemocyte-derived signaling promotes basal and damage- or infection-induced proliferation of intestinal stem cells in adults but failed to detect a larval gut phenotype after ablation of hemocytes with Hml^{Δ} (Ayyaz et al., 2015). The striking reduction in larval midgut length that we observed could indicate a similar developmental function of hemocytes, which was previously obscured by incomplete hemocyte ablation. However, we cannot exclude that lethality resulted from pleiotropic defects that we observed later in development.

A drawback of apoptosis-driven depletion of hemocytes is that the increase in apoptotic bodies may in itself induce a physiological response in the fly, including upregulation of immune-related genes (Arefin et al., 2015). In future studies it would be interesting to assess whether the genetic manipulation of specific hemocyte functions recapitulates pupal lethality, as seen when hemocyte migration is impaired in embryos (Matsubayashi et al., 2017).

MATERIALS AND METHODS

Drosophila melanogaster strains

Fly strains obtained from Bloomington Drosophila Stock Center were Hml^{Δ}-GAL4 (30139), *UAS-2xEGFP* (6874), *UAS-rpr* II (5824), *UAS-rpr* X (5823), *srp*Hemo-QF2 (78365), *srp*Hemo-GAL80 (78366), Hml^{Δ}-QF2 (66468), *QUAS*-GAL80 (51950), *QUAS*-mCherry (5227) and attP2 (8622). The *P{UAS-Bax.G}* integration on chromosome II (*UAS-Bax*) was a gift from Carla Saleh (Department of Virology, Institute Pasteur, Paris, France) and balanced with CyO, *P{ActGFP}JMR1*. The Hml^{P2A}-GAL4 lines were constructed in this study. Genotypes derived from these strains are listed in Table S2.

Generation of Hml^{P2A}-GAL4 Flies

A 3477 bp fragment was synthesized (Eurofins) containing 840 bp upstream of the *Hml* transcription start site and the *Hml* transcript up to the end of exon 9 (bp13845367-bp13848766, dm6), directly followed by an *Avr*II site, a P2A translation skip sequence and a *Xba*I site. The *Xba*I site was used to insert the GAL4 coding sequence from pGawB followed by a SV40 3′ untranslated region from pUASt. The construct was assembled in a backbone derived from pDESTR3R4-ϕ*C31att*B (Gunesdogan et al., 2010), containing a w^{+mc} transformation marker and attB integration sequence. Transgenic lines were generated in *P{CaryP}attP40* and *P{CaryP}attP2* by Rainbow Transgenics. The resulting *P{Hml-GAL4.P2A}attP40* and *P{Hml-GAL4.P2A}attP2* integrations were crossed out to remove integrase transgenes before further use.

Controlled density cultures

Cultures were raised on rich cornmeal molasses food (25 g Agar-Agar, 14.4 g yeast, 8 g soy flour, 64 g yellow cornmeal, 64 g light malt extract, 17.6 g molasses, 6 ml propionic acid, 0.8 g Nipagin/l). For GF cultures, medium was autoclaved before adding propionic acid. For antibiotic treatment, 5 mg/ml ampicillin (Sigma-Aldrich) +5 mg/ml kanamycin (Sigma-Aldrich) was added before pouring the food at ∼50°C. For controlled density cultures, embryos were collected on apple juice agar plates at 25°C in a 12 h light/dark cycling incubator. First instar larvae were picked from plates and seeded at 100 or 120 larvae per vial. Conventional/antibiotics cultures contained live yeast. For staged cultures, first instar larvae that hatched within a 5 h time window were seeded. Larvae were raised at 25°C in a 12 h light/dark cycling incubator.

Larval/pupal survival assays

For crosses involving *P{UAS-rpr.C}14*, larval survival was scored as fraction of pupae formed from seeded first instar larvae. For crosses involving *P{UAS-Bax.G}*, larval survival was scored relative to internal control genotype (Hml^{P2A}>*Bax* per Hml^{P2A}>*Bal*). For crosses involving *P{UAS-rpr.C}14*, pupal survival was scored as fraction of pupae that developed to adults (or a specific pupal stage) from all pupae that were formed in a vial. For crosses involving *P{UAS-Bax.G}*, pupal survival was scored as number of adults relative to internal control genotype (Hml^{P2A}>*Bax per* Hml^{P2A}>*Bal*). From this cross we expected 1:1 Hml^{P2A}>*Bax*:Hml^{P2A}>*Bal* adults if there was no effect in *Bax*-expressing animals. The fraction of expected therefore was scored relative to balancer carrying animals. As balancer chromosomes can, to some degree, reduce fitness, the fraction of expected can be higher than one in some cases. For analysis of pupariation timing, newly formed pupae were scored in 24 h intervals. Vials were left 1 week longer than eclosion was observed in control genotypes to check for late eclosing adults. All pupae that did not eclose were inspected and scored as light pupae (<stage P8), pharates (stage P8-P14) or failed eclosion (stage P15).

Germ-free cultures

Embryos were collected from crosses for 6 h at 25°C. Embryos were washed twice in a 100 µm cell-strainer with PBTx.01 [PBS, 0.01% Triton X-100 (Sigma-Aldrich)] and transferred to 70% ethanol in a clean bench. After 5 min, embryos were dechorionated in 50:50 Clorax/water (2.5% HOCl final) for 2 min and washed three times in sterile PBTx.01. For initial experiments (Fig. 2B; Fig. S4B) embryos were suspended in PBTx.01 and total number of embryos approximated by counting from an aliquot. An average of 100 embryos were seeded in sterile food vials by pipetting the respective amount of embryo suspension. For all other experiments, embryos were transferred to sterile agar plates and hatched larvae were picked for a time window of 5 h using a Lynx EVO stereomicroscope (Vision Engineering) in a clean bench. To check for GF conditions, five adults/pupae from each culture were homogenized in 100 µl PBS and plated on YPD. Plates were sealed and incubated for 3 days at 30°C. Plates from conventional conditions that were included with each plating showed a lawn of yeast/bacteria; GF cultures that showed any growth on plates were excluded from the analysis (<5% of cultures).

Hemocyte extraction by bleeding

Larvae were collected and extensively washed with water in 100 µm cell-strainers to remove debris followed by 5 min in 70% ethanol. Sessile hemocytes were dislodged by extensively rubbing the larvae with a paint brush. Larval cuticles were ripped open from posterior to anterior using fine forceps and hemocytes bled out.

Hemocyte quantification and staining

For hemocytometer counts, larvae were bled into 20 µl PBS, 5 mM EDTA, 1:250 protease inhibitor cocktail (Sigma-Aldrich) on parafilm. For antibody staining, five larvae were bled into 200 µl Schneider's medium (Sigma-Aldrich) with 10 mM N-Acetyl-L-Cysteine (Sigma-Aldrich) in eight-well µ-slide dishes (ibidi). Cells were allowed to adhere for 30 min, washed twice with Schneider's medium and fixed for 10 min with 4% paraformaldehyde (Sigma-Aldrich), 50 mM EDTA in PBS. Samples were washed with PBTx (PBS, 0.1% Triton X-100) and blocked for 30 min with 10% goat serum (Sigma-Aldrich) in PBTx (PBTx-GS). Primary antibodies 1:60 in PBTx-GS (anti-Nimrod C1 clones P1a/P1b, anti-Hemese clone H2, anti-Attila clones L1a/L1b/L1c, gift from Istvan Ando, Szeged, Hungary; Kurucz et al., 2007b) were incubated overnight at 4°C. After three washes with PBTx, samples were incubated with AlexaFluor 647 goat anti mouse (1:500, Abcam, ab150115) and 0.1 mg/ml RNase A (Sigma-Aldrich) in in PBTx-GS for 2 h at room temperature. After two washes with PBTx, samples were overlaid with 5 µM DAPI (Roth) in PBTx. Entire wells were scanned using a Leica SP8 confocal microscope and images analyzed in Fiji. For quantification of ablation experiments, images were first segmented based on antibody staining. Within antibody-positive area, segmentation based on DNA staining with particle limits 5-50 μm^2 was used to determine cell numbers. Lamellocytes were selected manually from scans of entire wells stained with anti-Hemese antibody and checked for a minimum single cell size of 300 μm^2, which was ∼2.5 times larger than the average size of Hemese-positive cells (∼120 μm^2). For quantification of co-expression,

Development (2022) 149, dev200286. doi:10.1242/dev.200286

images were segmented based on DNA staining with a lower area limit of 20 µm^2 and signal thresholds were adjustment to yield an average area of 55 µm^2 over all detections. Analysis was then limited to particle sizes between 28-83 µm^2. Within these regions, average signal intensities for EGFP, mCherry and Alexa 647 were measured. Thresholds for positive detections were set in R based on the analysis of signal histograms. For crystal cell quantification, larvae were picked and washed in PBS and then heat-shocked at 65°C for 10 min, which causes the crystal cells to melanize and turn black. For each larva, a dorsal and ventral image was taken using a Leica M205 stereomicroscope. Crystal cells were counted manually.

Hemocyte flow cytometry

For analysis of EGFP expression, 50 larvae were bled into the lid of a 1.5 ml Eppendorf tube containing 200 µl Schneider's medium, 1:250 protease inhibitor cocktail (Sigma-Aldrich). Carcasses were removed and the cell solution was transferred to a 1.5 ml Eppendorf tube containing 800 µl fresh Schneider's medium and passed through a 70 µm Flowmi tip filter (Sigma-Aldrich). Cells were analyzed on a MACSQuant Analyser (Miltenyi Biotec). For the analysis of tissue-associated hemocytes, 20 larvae were washed in water and homogenized in 1 ml of PBS with 20-30 strokes in a 1 ml loose fit Dounce. The suspensions were passed through a 40 µM cell-strainer by centrifugation into Schneider's medium containing 25% fetal calf serum (FCS), 2 mM EDTA at 1500 ***g*** for 10 min. The supernatant was discarded and the pellet resuspended in 1 ml Schneider's medium and analyzed using CytoFLEX (Beckman). Data were analyzed using FlowJo software.

Live imaging experiments

Imaging of embryos and larvae was performed in Frame-Seal Hybridization Slide Chambers (15×15 mm, BioRad) filled with a gel of 30% (w/v) OptiPrep (Sigma-Aldrich) and 30% (w/v) Pluronic F-127 (Sigma-Aldrich) in PBS on a glass slide closed with a coverslip. The gel was kept liquid at 4°C and solidified at room temperature. Embryos were dechorionated in 50:50 Clorax:water (2.5% HOCl final) for 3 min, washed with embryo saline (0.7% NaCl, 0.01% Triton X-100) and glued to the coverslip that sealed the chamber. Larvae were washed in embryo saline, anesthetized with ether according to published protocol (Kakanj et al., 2020) and glued to the slide side of the chamber. Adult flies were anesthetized with ether and glued to a glass slide. Imaging of adults and whole larvae was carried out using a Leica M205 stereomicroscope, embryos and larval details were imaged on a Leica SP8 confocal microscope.

Larval and pupal gut analysis

Larvae were washed in water and transferred to either Schneider's medium or PBS for dissection. Intact guts were allowed to contract for 30 min and fixed for 10 min in 4% paraformaldehyde, 50 mM EDTA in PBS. For determination of gut length, guts were mounted in fixative in Frame-Seal Hybridization Slide Chambers, imaged with a Leica M205 stereomicroscope and analyzed in Fiji. For fluorescent staining, guts were washed in PBTx and stained in PBTx, 1 mg/ml RNase A, 5 µM DAPI, 300 nM Alexa Fluor 647 Phalloidin (Thermo Fisher Scientific) for 30 min. Samples were mounted in Frame-Seal Hybridization Slide Chambers and imaged with a Leica SP8 confocal microscope. For electron microscopy, midguts were post-fixed with 2.5% glutaraldehyde (Electron Microscopy Sciences) and embedded in groups into small cubes of low melting agarose. These were then further post-fixed with 0.5% osmium-tetroxide and tannic acid, contrasted with uranyl-acetate, dehydrated in a graded ethanol series and infiltrated in Polybed (Polysciences). The cubes were placed in flat embedding molds with Polybed. After polymerization, the blocks were trimmed to the desired sectioning plane and sections were cut at 60 nm. Specimen were analyzed in a Zeiss LEO 906E transmission electron microscope, equipped with a side-mounted digital camera (Morada, SIS-Olympus), at 100 kV.

Plasmatocyte RNA-seq

OreR larvae were raised at controlled density as described above. Plasmatocytes were extracted as described above into complete media in tissue-culture-treated dishes (Schneider's medium with 10% FCS and 10 mM N-acetyl-L-cysteine). For each sample, 80 larvae were bled. The larval carcasses were then removed and the plasmatocytes were allowed to attach for 10-15 min. Afterwards, plasmatocytes were washed four times with PBS and lysed in 900 µl TRIzol. Samples were moved to fresh prespun phase lock heavy tubes (5PRIME) and 250 µl chloroform was added to each sample, mixed thoroughly and centrifuged (12,000 ***g***, room temperature, 15 min). The upper aqueous phase was moved to a fresh DNA LoBind tube and mixed with 550 µl isopropanol and 1 µl glycogen (20 mg/ml, RNAse free). Samples were mixed by inverting and then incubated for 30 min in the freezer at −20°C. Samples were centrifuged (16,000 ***g***, 4°C, 10 min) and the supernatant was removed carefully without disrupting the pellet. The pellet was resuspended in 100 µl ultra-pure water with 300 mM sodium acetate and 1 µl glycogen (20 mg/ml, RNAse free). Then 300 µl ethanol was added and the sample was incubated for 20 min at −20°C, centrifuged (16,000 ***g***, 4°C, 10 min) and the supernatant discarded. The pellet was washed twice by adding 1 ml 70% ethanol (prepared with ultra-pure water), each time spinning down the pellet (16,000 ***g***, 4°C, 3 min). Afterwards, all supernatant was drained and the pellet was dried until no liquid was visible. The pellet was then resuspended in 15 µl of ultra-pure water and stored at −80°C. Libraries from samples were generated at the Max Planck Genome Centre in Cologne, Germany, using the New England Biolabs Next Ultra II Directional RNA library kit with polyA mRNA enrichment from ∼100 ng total RNA. Libraries were pooled and sequenced to a minimum of 16 million uniquely mapped single end 150 bp reads per sample at the Max Planck Genome Centre.

Larval RNA-seq

Hml^{P2A}-GAL4 in attP2 or control *P{CaryP}attP2* males were crossed to *UAS-rpr* X virgins and larvae were raised as described above. Ten male WS-larvae were collected per sample across independent replicates and snap-frozen in liquid nitrogen. Larvae were transferred to Lysing Matrix E homogenization tubes with 1 ml of TRIzol and ruptured on high settings in a FastPrep tissue homogenizer (MP Biomedicals). The supernatant was transferred to a fresh tube and spun down for 2 min at maximum speed. Then 800 µl of the TRIzol sample was transferred to a fresh prespun phase lock heavy tube and 200 µl chloroform was added. Phases were separated by spinning at 12,000 ***g*** for 15 min at 4°C. The upper aqueous phase was transferred to a fresh tube and mixed with 500 µl isopropanol. The resulting mix was spun at 20,000 ***g*** for 15 min at 4°C. All supernatant was drained and the pellet resuspended in 30 µl DNAse solution (Ambicon, final concentration 0.2 U/µl) and incubated for 1 h at 37°C. RNA was purified using the RNeasy Plus kit (Qiagen) by adding 270 µl RTL buffer and isolated according the manufacturer's instructions. RNA concentration was determined by Nanodrop and integrity was checked by Bioanalyzer. Libraries from samples were generated at the Max Planck Genome Centre using the New England Biolabs Next Ultra II Directional RNA library kit with polyA mRNA enrichment from ∼100 ng total RNA. Libraries were pooled and sequenced to a minimum of 10 million uniquely mapped 2×75 bp paired end reads per sample at the Max Planck Genome Centre.

RNA data mapping and analysis

The reference genome fasta sequence file of the Berkeley *Drosophila* Genome Project assembly dm6 and the related gtf genome annotation file for dm6 of ensembl release 91 (dm6.91) were downloaded from ensembl (www.ensmbl.org) (Zerbino et al., 2018). A reference genome index was generated using dm6.91 using STAR-2.7.0e (Dobin et al., 2013) and used to map the fastq files. Quality control of RNA-seq mapping was performed using RSeQC (Zhang et al., 2021). All quality control files for FastQC, STAR mapping and RSeQC were aggregated and visualized using MultiQC (Ewels et al., 2016) and all data were checked to make sure the library and sequencing was of good quality. Once a dataset passed quality control, the gene level read counts were determined from bam files using the subread package (Liao et al., 2013). The gene level read counts were then loaded into R. For principal component analysis (PCA) the matrix of gene level read counts was transformed using the DESeq2 (Love et al., 2014) rlog function, from which the 1000 most-variant genes were selected. PCA was performed using the stats package prcomp function. For differential expression analysis, gene level read counts were processed using the edgeR package

(Robinson et al., 2010) with the quasi-likelihood general linear model approach according to the manual. GO Term enrichment was performed using GOrilla (http://cbl-gorilla.cs.technion.ac.il/) (Eden et al., 2009), testing enrichment of regulated protein coding gene sets against all genes detected in the experiment.

Tissue enrichment analysis

All available datasets for protein coding genes detected in the RNA-seq experiments were downloaded as text files from the web interface of FlyAtlas2 (http://flyatlas.gla.ac.uk/FlyAtlas2/index.html?page=home#). Tissue enrichments of individual transcripts were extracted from these files, leaving out the enrichment in Garland cells as no documentation was available on how these cells were purified. The enrichment values were scaled in R and the resulting *z*-scores visualized as heatmaps after k-means clustering.

Acknowledgements

The authors thank the Max Planck Sequencing Center in Cologne, Germany, for the library preparation and sequencing, Istvan Ando for the hemocyte antibodies and Carla Saleh for the UAS-*Bax* fly stock.

Competing interests

The authors declare no competing or financial interests.

Author contributions

Conceptualization: H.N.S., R.S., A.H.; Methodology: H.N.S., R.S., A.H., C.G.; Validation: H.N.S., R.S., F.G.; Formal analysis: H.N.S., R.S., A.H., F.G.; Investigation: H.N.S., R.S., A.H., F.G., C.G.; Data curation: H.N.S., R.S., A.H.; Writing - original draft: H.N.S.; Writing - review & editing: H.N.S., R.S., A.H., F.G.; Visualization: H.N.S., R.S., A.H.; Supervision: A.H.; Project administration: H.N.S., A.H.

Funding

All of the authors were supported by core funding from the Max-Planck-Gesellschaft. Open Access funding provided by the Max Planck Society. Deposited in PMC for immediate release.

Data availability

RNA-seq data of hemocyte-ablated larvae and of primary plasmatocytes are available on ArrayExpress (E-MTAB-11095 and E-MTAB-10759, respectively).

Peer review history

The peer review history is available online at https://journals.biologists.com/dev/lookup/doi/10.1242/dev.200286.reviewer-comments.pdf.

References

Arefin, B., Kucerova, L., Krautz, R., Kranenburg, H., Parvin, F. and Theopold, U. (2015). Apoptosis in hemocytes induces a shift in effector mechanisms in the Drosophila immune system and leads to a pro-inflammatory state. *PLoS One* **10**, e0136593. doi:10.1371/journal.pone.0136593

Ayyaz, A., Li, H. and Jasper, H. (2015). Haemocytes control stem cell activity in the Drosophila intestine. *Nat. Cell Biol.* **17**, 736-748. doi:10.1038/ncb3174

Bainbridge, S. P. and Bownes, M. (1981). Staging the metamorphosis of Drosophila melanogaster. *J. Embryol. Exp. Morphol.* **66**, 57-80.

Binggeli, O., Neyen, C., Poidevin, M. and Lemaitre, B. (2014). Prophenoloxidase activation is required for survival to microbial infections in Drosophila. *PLoS Pathog.* **10**, e1004067. doi:10.1371/journal.ppat.1004067

Braun, A., Hoffmann, J. A. and Meister, M. (1998). Analysis of the Drosophila host defense in domino mutant larvae, which are devoid of hemocytes. *Proc. Natl. Acad. Sci. USA* **95**, 14337-14342. doi:10.1073/pnas.95.24.14337

Bruckner, K., Kockel, L., Duchek, P., Luque, C. M., Rørth, P. and Perrimon, N. (2004). The PDGF/VEGF receptor controls blood cell survival in Drosophila. *Dev. Cell* **7**, 73-84. doi:10.1016/j.devcel.2004.06.007

Cattenoz, P. B., Sakr, R., Pavlidaki, A., Delaporte, C., Riba, A., Molina, N., Hariharan, N., Mukherjee, T. and Giangrande, A. (2020). Temporal specificity and heterogeneity of Drosophila immune cells. *EMBO J.* **39**, e104486. doi:10.15252/embj.2020104486

Charroux, B. and Royet, J. (2009). Elimination of plasmatocytes by targeted apoptosis reveals their role in multiple aspects of the Drosophila immune response. *Proc. Natl. Acad. Sci. USA* **106**, 9797-9802. doi:10.1073/pnas.0903971106

Coates, J. A., Brooks, E., Brittle, A. L., Armitage, E. L., Zeidler, M. P. and Evans, I. R. (2021). Identification of functionally distinct macrophage subpopulations in Drosophila. *eLife* **10**, e58686. doi:10.7554/eLife.58686

Cox, N., Crozet, L., Holtman, I. R., Loyher, P. L., Lazarov, T., White, J. B., Mass, E., Stanley, E. R., Elemento, O., Glass, C. K. et al. (2021). Diet-regulated production of PDGFcc by macrophages controls energy storage. *Science* **373**, eabe9383. doi:10.1126/science.abe9383

Das, D., Ashoka, D., Aradhya, R. and Inamdar, M. (2008). Gene expression analysis in post-embryonic pericardial cells of Drosophila. *Gene Expr. Patterns* **8**, 199-205. doi:10.1016/j.gep.2007.10.008

Defaye, A., Evans, I., Crozatier, M., Wood, W., Lemaitre, B. and Leulier, F. (2009). Genetic ablation of Drosophila phagocytes reveals their contribution to both development and resistance to bacterial infection. *J. Innate Immun.* **1**, 322-334. doi:10.1159/000210264

Dobin, A., Davis, C. A., Schlesinger, F., Drenkow, J., Zaleski, C., Jha, S., Batut, P., Chaisson, M. and Gingeras, T. R. (2013). STAR: ultrafast universal RNA-seq aligner. *Bioinformatics* **29**, 15-21. doi:10.1093/bioinformatics/bts635

Eden, E., Navon, R., Steinfeld, I., Lipson, D. and Yakhini, Z. (2009). GOrilla: a tool for discovery and visualization of enriched GO terms in ranked gene lists. *BMC Bioinformatics* **10**, 48. doi:10.1186/1471-2105-10-48

Ewels, P., Magnusson, M., Lundin, S. and Käller, M. (2016). MultiQC: summarize analysis results for multiple tools and samples in a single report. *Bioinformatics* **32**, 3047-3048. doi:10.1093/bioinformatics/btw354

Gunesdogan, U., Jäckle, H. and Herzig, A. (2010). A genetic system to assess in vivo the functions of histones and histone modifications in higher eukaryotes. *EMBO Rep.* **11**, 772-776. doi:10.1038/embor.2010.124

Gyoergy, A., Roblek, M., Ratheesh, A., Valoskova, K., Belyaeva, V., Wachner, S., Matsubayashi, Y., Sanchez-Sanchez, B. J., Stramer, B. and Siekhaus, D. E. (2018). Tools allowing independent visualization and genetic manipulation of drosophila melanogaster macrophages and surrounding tissues. *G3* **8**, 845-857. doi:10.1534/g3.117.300452

Jung, S. H., Evans, C. J., Uemura, C. and Banerjee, U. (2005). The Drosophila lymph gland as a developmental model of hematopoiesis. *Development* **132**, 2521-2533. doi:10.1242/dev.01837

Kakanj, P., Eming, S. A., Partridge, L. and Leptin, M. (2020). Long-term in vivo imaging of Drosophila larvae. *Nat. Protoc.* **15**, 1158-1187. doi:10.1038/s41596-019-0282-z

Kurucz, E., Zettervall, C. J., Sinka, R., Vilmos, P., Pivarcsi, A., Ekengren, S., Hegedus, Z., Ando, I. and Hultmark, D. (2003). Hemese, a hemocyte-specific transmembrane protein, affects the cellular immune response in Drosophila. *Proc. Natl. Acad. Sci. USA* **100**, 2622-2627. doi:10.1073/pnas.0436940100

Kurucz, E., Markus, R., Zsamboki, J., Folkl-Medzihradszky, K., Darula, Z., Vilmos, P., Udvardy, A., Krausz, I., Lukacsovich, T., Gateff, E. et al. (2007a). Nimrod, a putative phagocytosis receptor with EGF repeats in Drosophila plasmatocytes. *Curr. Biol.* **17**, 649-654. doi:10.1016/j.cub.2007.02.041

Kurucz, E., Vaczi, B., Márkus, R., Laurinyecz, B., Vilmos, P., Zsámboki, J., Csorba, K., Gateff, E., Hultmark, D. and Andó, I. (2007b). Definition of Drosophila hemocyte subsets by cell-type specific antigens. *Acta Biol. Hung.* **58**, 95-111. doi:10.1556/ABiol.58.2007.Suppl.8

Leader, D. P., Krause, S. A., Pandit, A., Davies, S. A. and Dow, J. A. T. (2018). FlyAtlas 2: a new version of the Drosophila melanogaster expression atlas with RNA-Seq, miRNA-Seq and sex-specific data. *Nucleic Acids Res.* **46**, D809-D815. doi:10.1093/nar/gkx976

Leitao, A. B. and Sucena, E. (2015). Drosophila sessile hemocyte clusters are true hematopoietic tissues that regulate larval blood cell differentiation. *eLife* **4**, e06166. doi:10.7554/eLife.06166

Liao, Y., Smyth, G. K. and Shi, W. (2013). The Subread aligner: fast, accurate and scalable read mapping by seed-and-vote. *Nucleic Acids Res.* **41**, e108. doi:10.1093/nar/gkt214

Love, M. I., Huber, W. and Anders, S. (2014). Moderated estimation of fold change and dispersion for RNA-seq data with DESeq2. *Genome Biol.* **15**, 550. doi:10.1186/s13059-014-0550-8

Mase, A., Augsburger, J. and Bruckner, K. (2021). Macrophages and their organ locations shape each other in development and homeostasis - a Drosophila perspective. *Front. Cell Dev. Biol.* **9**, 630272. doi:10.3389/fcell.2021.630272

Matsubayashi, Y., Louani, A., Dragu, A., Sánchez-Sánchez, B. J., Serna-Morales, E., Yolland, L., Gyoergy, A., Vizcay, G., Fleck, R. A., Heddleston, J. M. et al. (2017). A moving source of matrix components is essential for De Novo basement membrane formation. *Curr. Biol.* **27**, 3526-3534.e4. doi:10.1016/j.cub.2017.10.001

Nehme, N. T., Quintin, J., Cho, J. H., Lee, J., Lafarge, M. C., Kocks, C. and Ferrandon, D. (2011). Relative roles of the cellular and humoral responses in the Drosophila host defense against three gram-positive bacterial infections. *PLoS One* **6**, e14743. doi:10.1371/journal.pone.0014743

Olofsson, B. and Page, D. T. (2005). Condensation of the central nervous system in embryonic Drosophila is inhibited by blocking hemocyte migration or neural activity. *Dev. Biol.* **279**, 233-243. doi:10.1016/j.ydbio.2004.12.020

Robinson, M. D., Mccarthy, D. J. and Smyth, G. K. (2010). edgeR: a bioconductor package for differential expression analysis of digital gene expression data. *Bioinformatics* **26**, 139-140. doi:10.1093/bioinformatics/btp616

Shia, A. K., Glittenberg, M., Thompson, G., Weber, A. N., Reichhart, J. M. and Ligoxygakis, P. (2009). Toll-dependent antimicrobial responses in Drosophila

larval fat body require Spatzle secreted by haemocytes. *J. Cell Sci.* **122**, 4505-4515. doi:10.1242/jcs.049155

Sinenko, S. A. and Mathey-Prevot, B. (2004). Increased expression of Drosophila tetraspanin, Tsp68C, suppresses the abnormal proliferation of ytr-deficient and Ras/Raf-activated hemocytes. *Oncogene* **23**, 9120-9128. doi:10.1038/sj.onc.1208156

Sinenko, S. A., Shim, J. and Banerjee, U. (2011). Oxidative stress in the haematopoietic niche regulates the cellular immune response in Drosophila. *EMBO Rep.* **13**, 83-89. doi:10.1038/embor.2011.223

Tattikota, S. G., Cho, B., Liu, Y., Hu, Y., Barrera, V., Steinbaugh, M. J., Yoon, S. H., Comjean, A., Li, F., Dervis, F. et al. (2020). A single-cell survey of Drosophila blood. *eLife* **9**, e54818. doi:10.7554/eLife.54818

Tepass, U., Fessler, L. I., Aziz, A. and Hartenstein, V. (1994). Embryonic origin of hemocytes and their relationship to cell death in Drosophila. *Development* **120**, 1829-1837. doi:10.1242/dev.120.7.1829

Zerbino, D. R., Achuthan, P., Akanni, W., Amode, M. R., Barrell, D., Bhai, J., Billis, K., Cummins, C., Gall, A., Giron, C. G. et al. (2018). Ensembl 2018. *Nucleic Acids Res.* **46**, D754-D761. doi:10.1093/nar/gkx1098

Zhang, T., Singh, J., Litfin, T., Zhan, J., Paliwal, K. and Zhou, Y. (2021). RNAcmap: a fully automatic pipeline for predicting contact maps of RNAs by evolutionary coupling analysis. *Bioinformatics* **37**, 3494-3500. doi:10.1093/bioinformatics/btab391

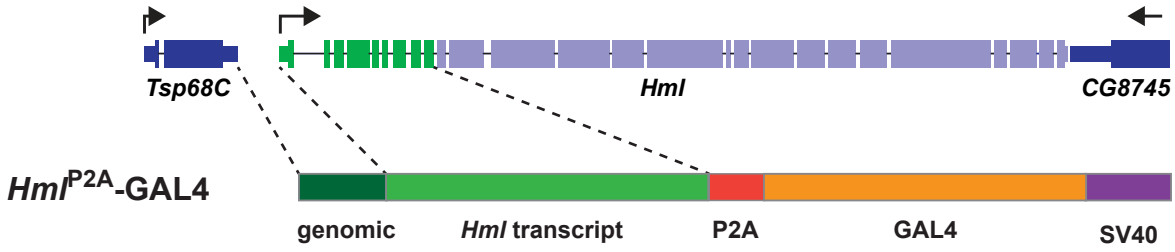

Fig. S1. Schematic of the *Hml* gene and the *Hml*^{P2A}-GAL4 construct.

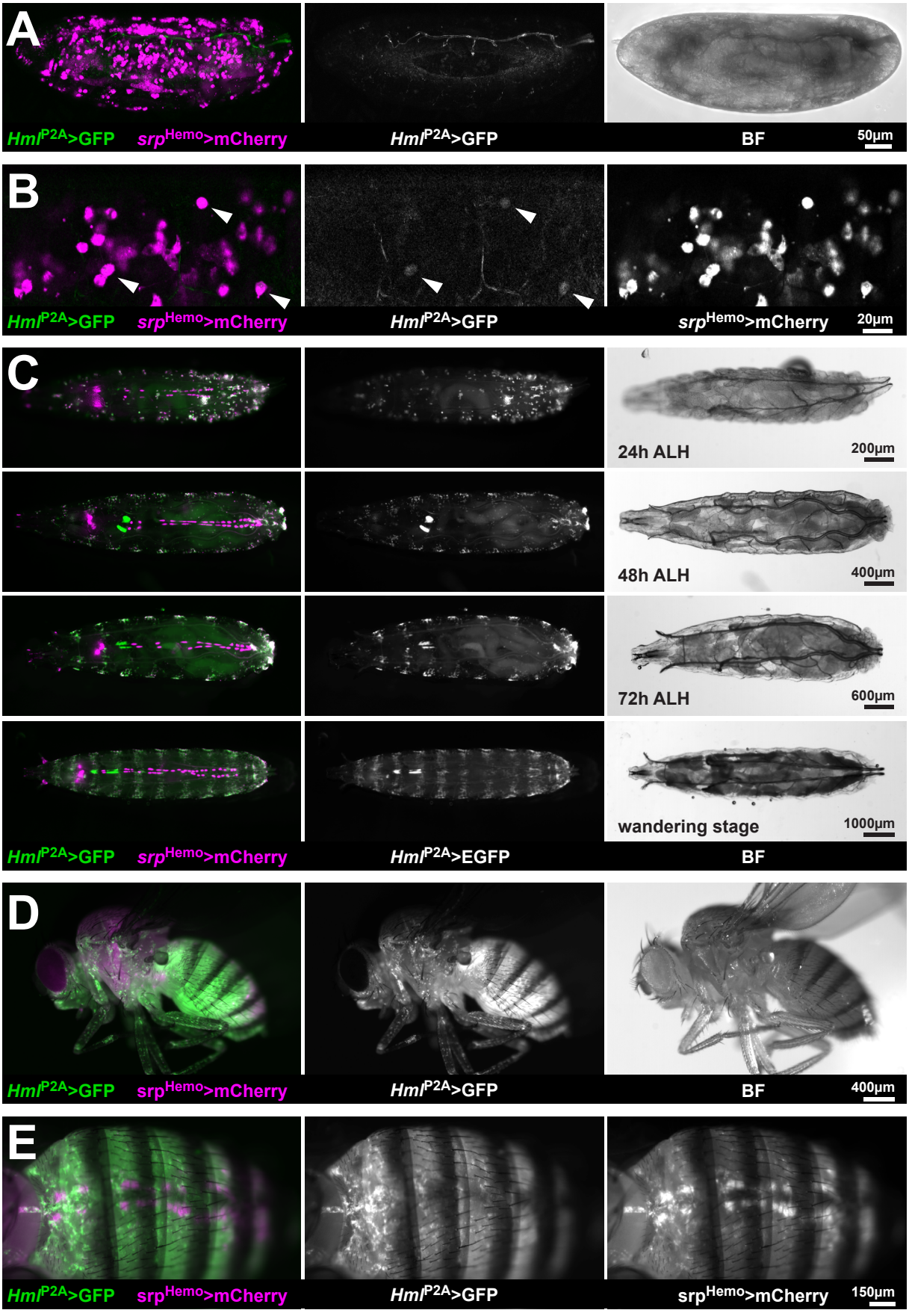

Fig. S2. (A-E) Fluorescent live imaging of *Hml*^{P2A}>GFP (attP40); *srp*Hemo>mCherry animals reared under conventional conditions and controlled density (B-E).

(A) Maximum projection of an image stack that included ~80µm from the apical surface of a stage 17 embryo briefly before hatching, as indicated by air filled trachea.

(B) Maximum projection of the hemocytes containing apical region of the embryo shown in (A). Arrowheads mark hemocytes with faint expression of *Hml*^{P2A}>GFP.

(C) Dorsal view of whole larvae in a time course of late first instar (24h after larval hatching, ALH), late second instar (48 h ALH), mid third instar (72 h ALH) and WS-larvae (wandering stage). BF indicates bright field images. Outside hemocytes, *srp*Hemo>mCherry is detected in some cells of unknown identity at the anterior of larva (left), in Garland cells that form a group of cells in the interior at about 20% larval length close to the brain, and in pericardial nephrocytes that form two rows of cells along the heart at the dorsal midline. We did not detect *Hml*^{P2A}>GFP expression in any of these regions.

(D & E) Whole mount female fly (D) and close up of the abdomen of a female fly showing expression of *srp*^{Hemo}>mCherry in adult pericardial nephrocytes (E).

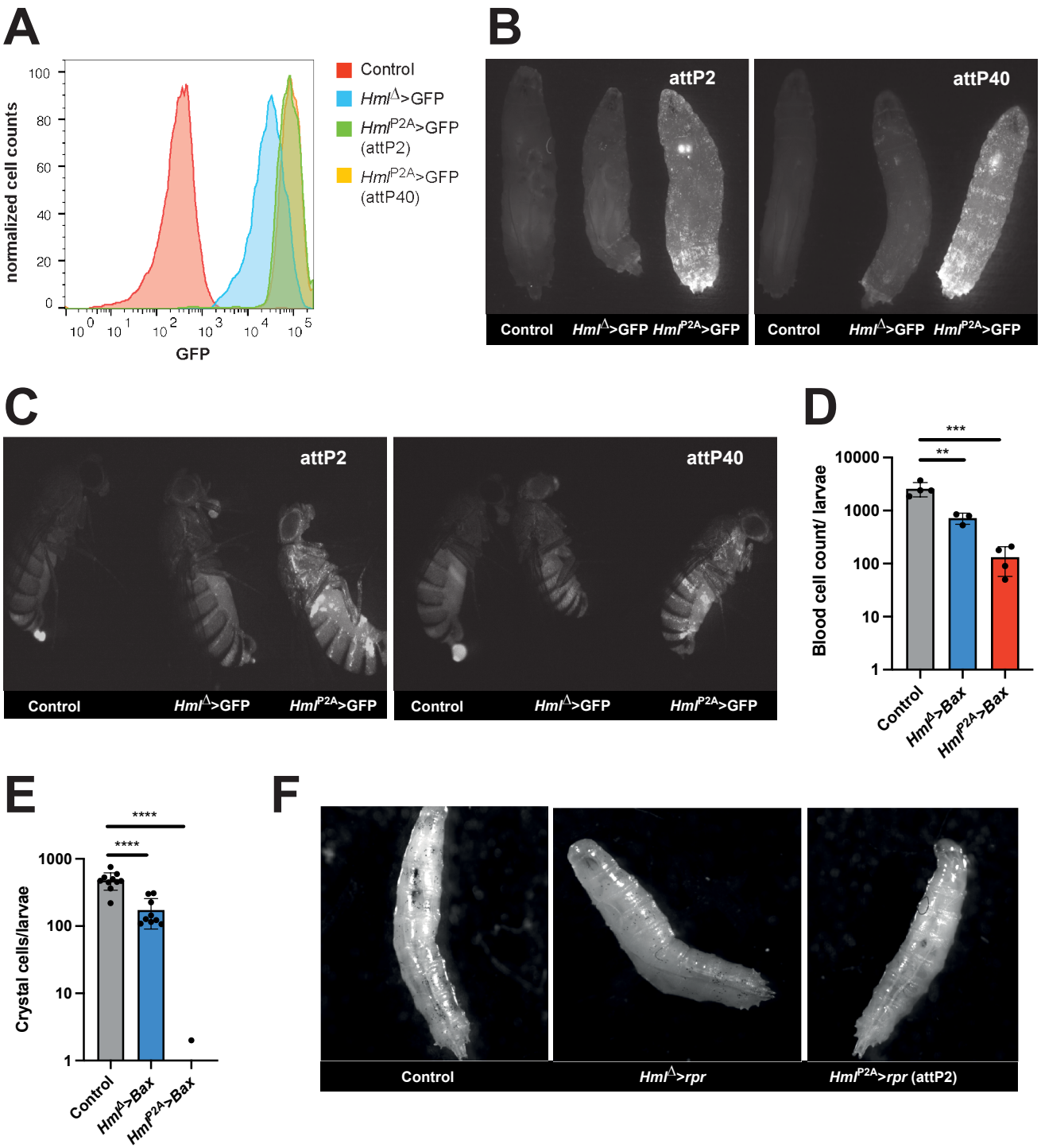

Fig. S3. (A) Flow cytometry analysis of extracted hemocytes from WS-larvae comparing the expression of *Hml*$^{\Delta}$>GFP, *Hml*^{P2A}>GFP (attP2) and *Hml*^{P2A}>GFP (attP40). Representative histogram from two independent experiments.

(B) Whole mount fluorescence microscopy of WS-larvae comparing the expression of *Hml*$^{\Delta}$>GFP to *Hml*^{P2A}>GFP (attP2; left) and Hml$^{\Delta}$>GFP to Hml^{P2A}>GFP (attP40; right). Representative images from two independent experiments.

(C) Whole mount fluorescence microscopy of adult females comparing the expression of *Hml*$^{\Delta}$>GFP to *Hml*^{P2A}>GFP (attP2; left) and *Hml*$^{\Delta}$>GFP to *Hml*^{P2A}>GFP (attP40; right). Representative images from two independent experiments.

(D) Blood cell counts by hemocytometer of hemocytes from WS-larvae from *Bax* mediated ablation in *Hml*$^{\Delta}$>*Bax* or *Hml*^{P2A}>*Bax* (attP2). One-way ANOVA was performed

(E) Crystal cell counts by whole mount microscopy of WS-larvae after *Bax* mediated ablation in *Hml*$^{\Delta}$>*Bax* or *Hml*^{P2A}>*Bax* (attP2). Each dot represents counts from a single animal. One-way ANOVA was performed.

(F) Representative images of *Hml*$^{\Delta}$>*rpr* or *Hml*^{P2A}>*rpr* (attP2) WS-larvae used for crystal cell quantification.

Data are mean±s.d. (D,E).

Controls: attP2>GFP (A-C), attP2>*rpr* (D & E), attP2>*rpr* (F).

** p<0.002; *** p<0.0002; **** p<0.0001

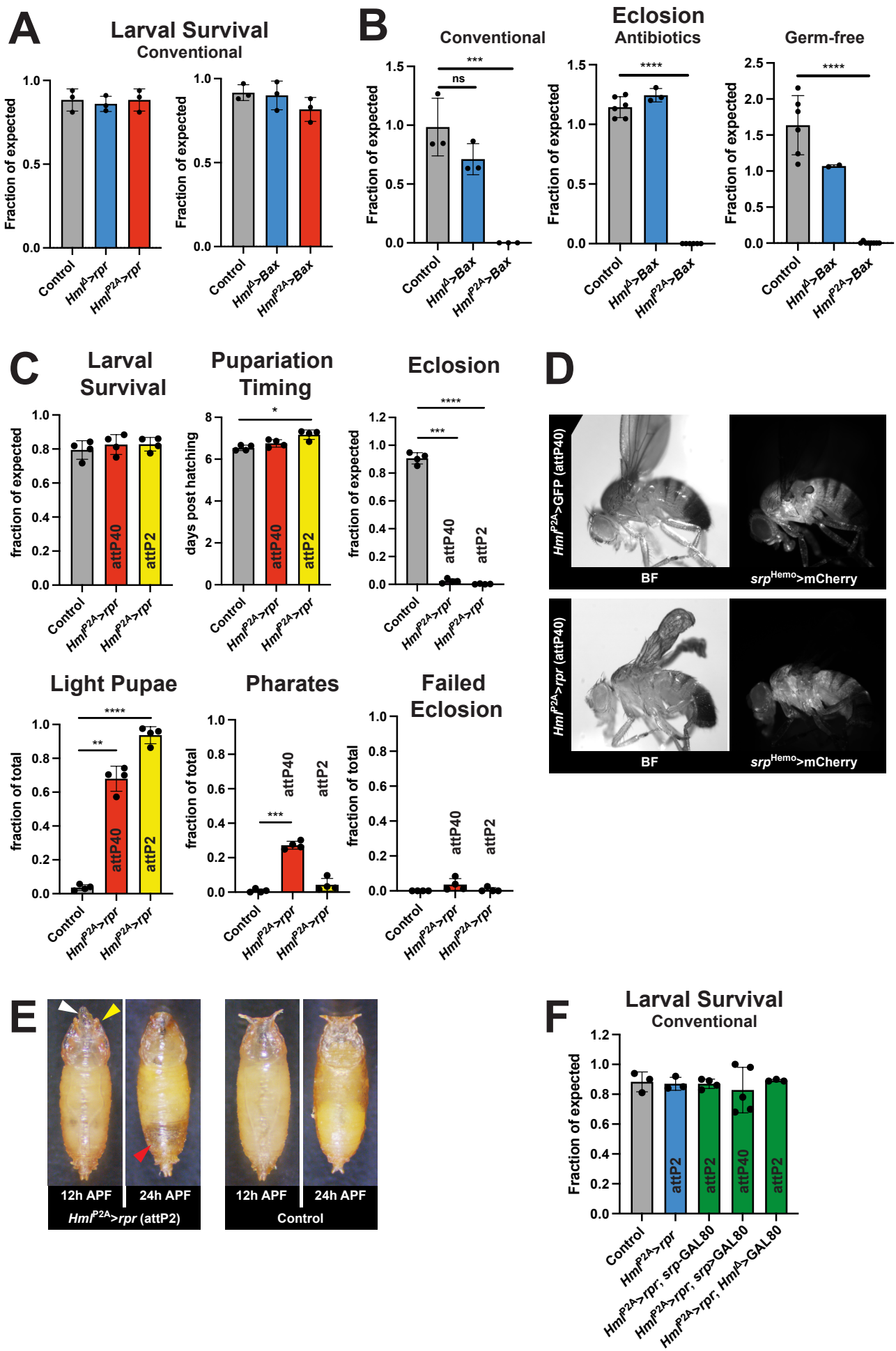
A
Larval Survival
Conventional
Fraction of expected
Control
Hml^Δ>rpr
Hml^P2A>rpr
Hml^Δ>Bax
Hml^P2A>Bax
B
Eclosion
Conventional
Antibiotics
Germ-free
***
ns
****
C
Larval Survival
Pupariation Timing
Eclosion
fraction of expected
days post hatching
attP40
attP2
Light Pupae
Pharates
Failed Eclosion
fraction of total
D
Hml^P2A>GFP (attP40)
Hml^P2A>rpr (attP40)
BF
srp^Hemo>mCherry
E
12h APF
24h APF
Hml^P2A>rpr (attP2)
Control
F
Larval Survival
Conventional
Hml^P2A>rpr; srp-GAL80
Hml^P2A>rpr; srp>GAL80
Hml^P2A>rpr; Hml^Δ>GAL80

Fig. S4. (A) Larval survival from controlled density cultures under conventional conditions. Survival was scored as pupae obtained from inoculated first instar larvae for *Hml*$^{\Delta}$>*rpr* or *Hml*^{P2A}>*rpr* (attP2). For *Hml*$^{\Delta}$>*Bax* or *Hml*^{P2A}>*Bax* (attP2) survival was scored relative to the internal controls *Hml*$^{\Delta}$>*Bal* or *Hml*^{P2A}>*Bal* as fraction of GFP negative per GFP positive pupae (see materials and methods section for details). Each dot represents an individual vial. One-way ANOVA were performed.

(B) Eclosion rates from *Hml*$^{\Delta}$>*Bax* or *Hml*^{P2A}>*Bax* (attP2) animals reared at controlled density under conventional conditions, on food containing 5 mg/mL Ampicillin and 5 mg/mL Kanamycin or under germ-free conditions. Eclosion rates were scored relative to the internal controls *Hml*$^{\Delta}$>*Bal* or *Hml*^{P2A}>*Bal* as fraction of Cy+ per Cy- adults, which can produce fractions of expected >1 (see materials and methods section for details). Each dot represents an individual vial. One-way ANOVA were performed.

(C) Comparison of *Hml*^{P2A}-GAL4 driver inserted in attP40 or attP2 based on controlled density cultures raised under conventional conditions. Larval survival was scored as pupae obtained from inoculated first instar larvae. Eclosion rates were scored as number adults obtained from pupae that were formed and pupariation timing as average over the day of pupariation for each pupae in one vial. Pupal lethality was scored by determining the fraction of all pupae in a vial that terminated development before pupal stage P8 (light pupae), during stage P8-P14 (pharates) or in P15 (failed eclosion). Each dot represents an independent experiment including 4 vials each. One-way ANOVA were performed.

(D) Representative whole mount images of *Hml*^{P2A}>GFP (attP40), *srp*^{Hemo}>mCherry animals (top) and surviving *Hml*^{P2A}>*rpr* (attP40), *srp*^{Hemo}>mCherry animals. *Hml*^{P2A}>*rpr* (attP40), *srp*Hemo>mCherry animals still contained *srp*^{Hemo}>mCherry and showed a wing inflation phenotype.

(E) Pupal phenotypes of *Hml*^{P2A}>*rpr* (attP2) animals. In early pupae (12h after pupariation formation) defective retraction of mouth hooks (white arrowhead) and lack of clearly visible anterior spiracles (yellow arrowhead) is evident. By 24 h after pupariation formation 95% of pupae show a large posterior air bubble (red arrowhead).

(F) Larval survival from controlled density cultures under conventional conditions. Survival was scored as pupae obtained from inoculated first instar larvae. Genotypes used here are identical with those in Figure 3F. One-way ANOVA were performed.

Data are mean±s.d.. Controls: attP2>*rpr* and attP2>Bax (A), attP2>Bax (B), yw>*rpr* (C & E), attP2>*rpr* (F). * $p<0.03$; ** $p<0.002$; *** $p<0.0002$; **** $p<0.0001$. ns, not significant.

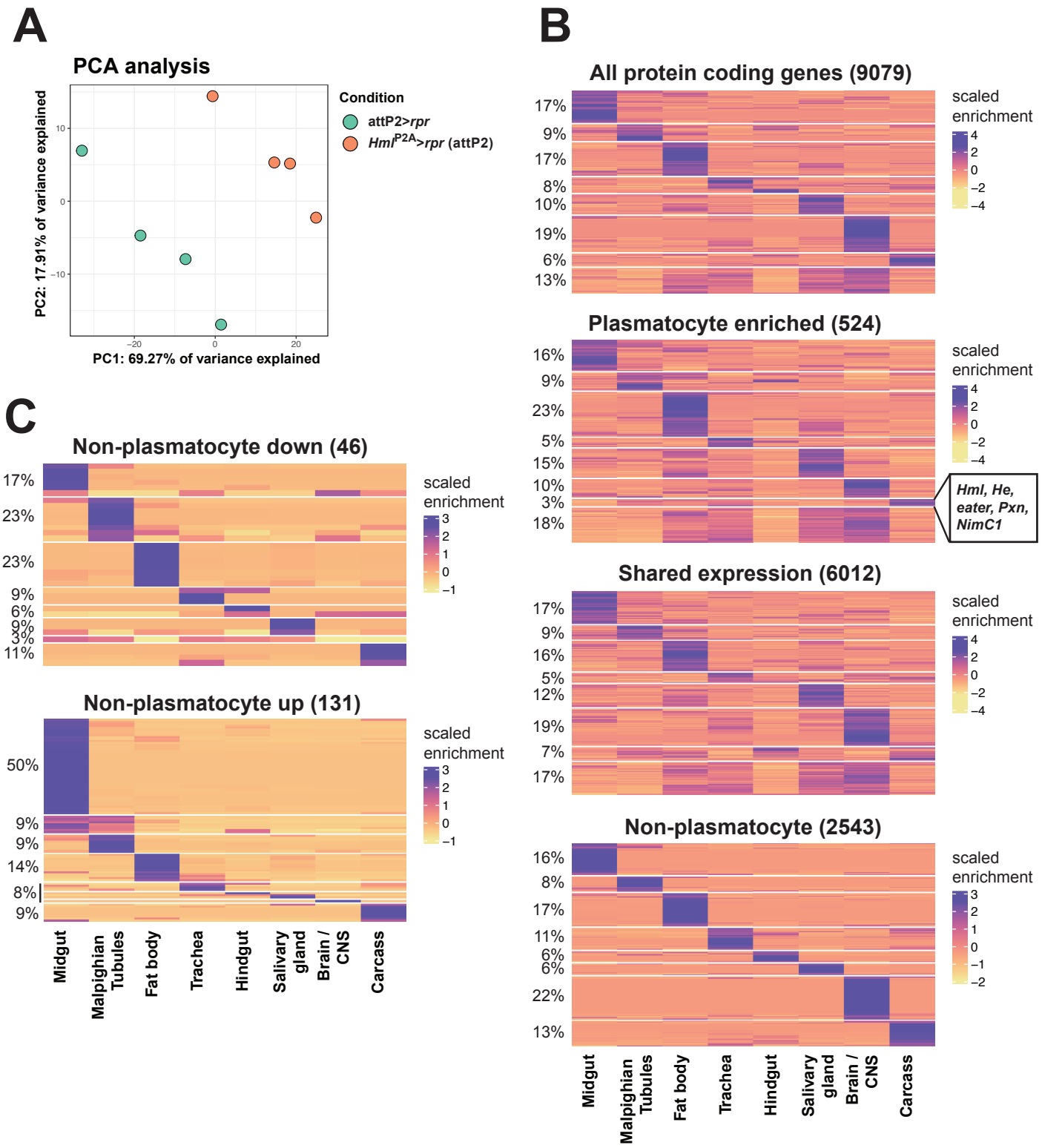

Fig. S5. (A) Principle component analysis (PCA) of RNAseq replicate data from *Hml*^{P2A}*>rpr* and *attP2>rpr* WS-larvae. Samples of both genotypes are separated by a shared component in PC1 and PC2, suggesting a consistent transcriptional effect between replicates.
(B) Heatmap showing scaled tissue enrichment of all protein coding transcripts detected in our differential expression analysis for which data was available at FlyAtlas2 (All protein coding genes) and for subsets identified by our RNAseq analysis as plasmatocyte-enriched, shared or non-plasmatocyte expressed with the number of transcripts in brackets. Known plasmatocyte specific transcripts, which are part of the plasmatocyte enriched subset, show tissue enrichment in the carcass. The percentage of transcripts that are in each k means cluster of the heatmaps is indicated to the left.
(C) Heatmap showing scaled tissue enrichment of protein coding transcripts that were downregulated and classified as non-plasmatocyte expressed (upper panel) or upregulated and classified as non-plasmatocyte expressed (lower panel). Transcript numbers are indicated by brackets and the percentage of transcripts that are in each k means cluster of the heatmaps is indicated to the left.

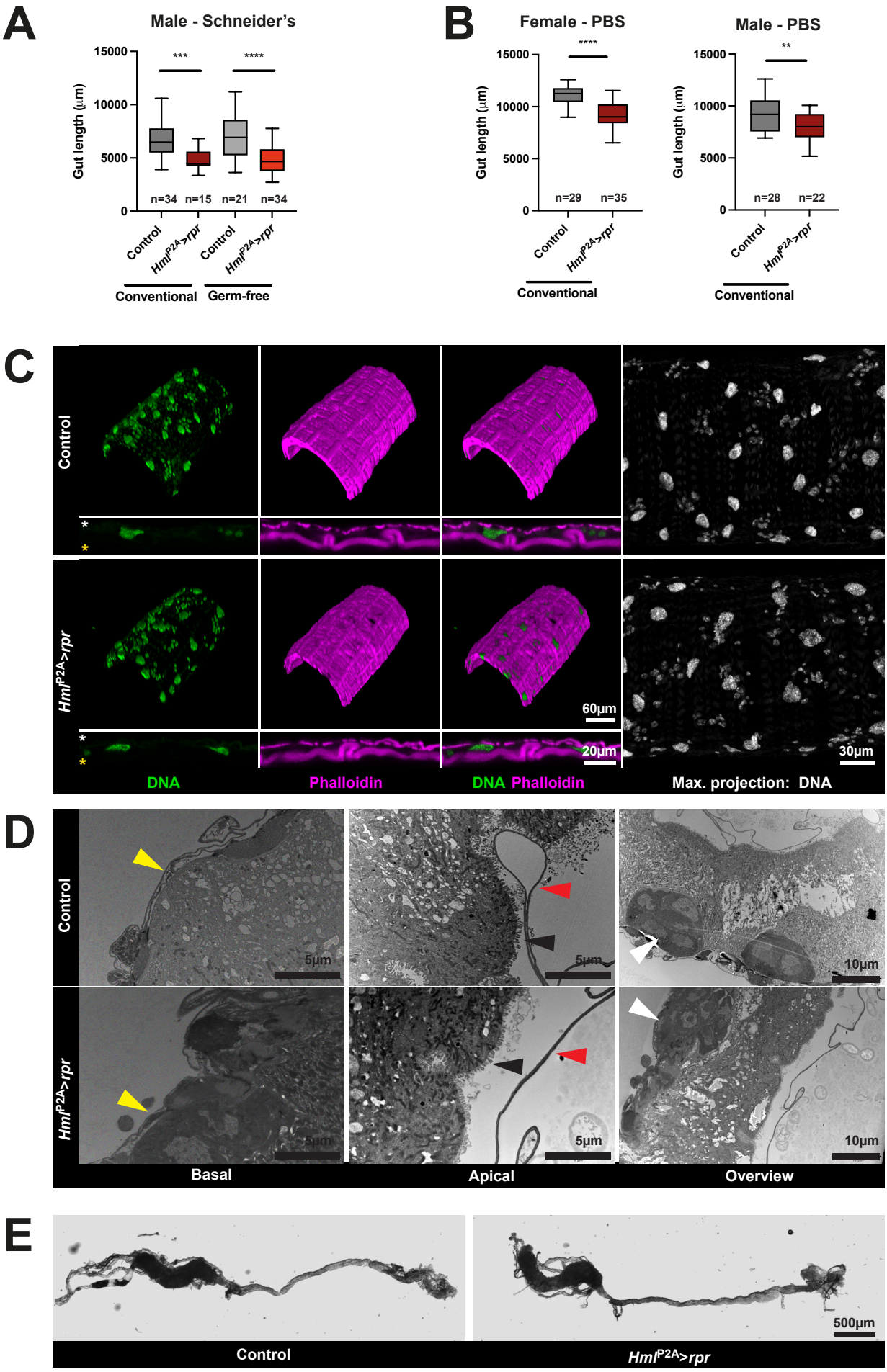

Fig. S6. (A & B) Midgut lengths from WS-larvae reared at controlled density were determined as outlined in Figure 4D. Dissection was carried out in Schneider's medium containing Ca^{2+} (A) or in calcium-free PBS (B), which reduced the contraction of guts after dissection. In both conditions, *Hml*^{P2A}>*rpr* (attP2) animals showed reduced midgut length compared to controls. This effect was observed despite the sexual dimorphism of midgut length in males and females and under conventional as well as germfree conditions. Number of guts are indicated. One-way ANOVA were performed. Box plot shows median values (middle bars) and first to third interquartile ranges (boxes); whiskers indicate minimum and maximum values.

(C). Fluorescent micrographs of midgut regions close to the midgut/hindgut border from *Hml*^{P2A}>*rpr* (attP2) and control WS-larvae reared at controlled density under conventional conditions and dissected in PBS. 3D reconstruction of DNA and Phalloidine staining consistently showed a slight deterioration of visceral musculature. In optical cross sections we observed no difference in staining the musculature on the basal side (white asterisk) and the brush border on the apical side of gut cells (yellow asterisk). Maximum projection of stacks visualized in 3D showed that enterocytes (large nuclei) and smaller cells that might include intestinal stem cells, enteroblasts and enterendocrine cells were present with no apparent differences.

(D) Electron micrographs of midgut regions close to the midgut/hindgut border from *Hml*^{P2A}>*rpr* (attP2) and control WS-larvae reared at controlled density under germ-free conditions. Basement membrane (yellow arrowheads), peritrophic membrane (red arrowheads) and microvilli (black arrowheads) are comparable between the genotypes.

(E) Brightfield images of pupal guts dissected from *Hml*^{P2A}>*rpr* (attP2) 24 h after pupariation and control pupae at 12h after pupariation.

Controls: yw>*rpr* (A-E). ** p<0.002; *** p<0.0002; **** p<0.0001

Table S1. RNA-seq data from HmlP2A>rpr (attP2) compared with attP2>rpr WS-larvae.
Genes were classified as non-plasmatocyte (no or marginal expression in plasmatocytes), shared or plasmatocyte-enriched (>4 fold elevated in plasmatocytes).

Click here to download Table S1

Table S2. Genotypes derived from fly strains.

***reaper*-mediated ablation**
Hml*^{P2A}>*rpr* (attP2)**: *w*/w^{1118}; P{UAS-rpr.C}14/+; P{Hml-GAL4.P2A}attP2/+* ***Hml*^{P2A}>*rpr* (attP40)**: *w*/w^{1118}; P{UAS-rpr.C}14/ P{Hml-GAL4.P2A}attP40; +/+* ***Hml*^{P2A}>*rpr* (attP40); *srp*^{Hemo}>*mCherry: *w*/w^{1118}; P{UAS-rpr.C}14/ P{Hml-GAL4.P2A}attP40;* *P{10XQUAS-6XmCherry-HA}attP2/M{srpHemo-QF2}ZH-86Fb* ***HmlΔ>rpr***: *w*/w^{1118}; P{UAS-rpr.C}14/ P{Hml-GAL4.Delta}2; +/+*
***Bax*-mediated ablation**
Hml*^{P2A}>*Bax* (attP2)**: *w*/w^{1118}; P{UAS-Bax.G} /+; P{Hml-GAL4.P2A}attP2/+* ***Hml*^{P2A}>*Bal* (attP2), internal control genotype GFP+ and Cy-**: *w*/w^{1118};* CyO, *P{ActGFP}JMR1/+; P{Hml-GAL4.P2A}attP2/+* ***HmlΔ>Bax: *w*/w^{1118}; P{UAS-Bax.G}/P{Hml-GAL4.Delta}2; +/+* ***HmlΔ>Bal*, internal control genotype GFP+ and Cy-**: *w*/w^{1118};* CyO, *P{ActGFP}JMR1/P{Hml-GAL4.Delta}2; +/+*
Expression analysis
Hml*^{P2A}>*GFP* (attP2)**: *w*/w*; P{ UAS-2xEGFP}AH2/+; P{Hml-GAL4.P2A}attP2/+* ***Hml*^{P2A}>*GFP* (attP40)**: *w*/w*; P{ UAS-2xEGFP}AH2/ P{Hml-GAL4.P2A}attP40; +/+* ***Hml*^{P2A}>*GFP* (attP40); *srp*^{Hemo}>*mCherry: *w*/w*; P{ UAS-2xEGFP}AH2/ P{Hml-GAL4.P2A}attP40;* *P{10XQUAS-6XmCherry-HA}attP2/M{srpHemo-QF2}ZH-86Fb* ***HmlΔ>GFP***: *w*/w*; P{ UAS-2xEGFP}AH2/P{Hml-GAL4.Delta}2; +/+*

Genetic rescue experiments
Hml*^{P2A}*>rpr* (attP2); *srp*^{Hemo}*-GAL80: *w*/w*; P{UAS-rpr.C}14/ +;* *P{Hml-GAL4.P2A}attP2/M{ srpHemo-GAL80}ZH-86Fb* ***Hml*^{P2A}*>rpr* (attP2); *Hml*Δ*>GAL80***: *w*/w*; P{UAS-rpr.C}14/P{Hml-QF2.Delta.L}2;* *P{QUAS-GAL80.P}28/ P{Hml-GAL4.P2A}attP2* ***Hml*^{P2A}*>rpr* (attP40); *srp*^{Hemo}*>GAL80***: *w*/w*; P{UAS-rpr.C}14/ P{Hml-GAL4.P2A}attP40;* *P{QUAS-GAL80.P}28/M{srpHemo-QF2}ZH-86Fb*
Control genotypes
***attP2>rpr* (attP2)**: *w*/ y^1 w^{67c23}; P{UAS-rpr.C}14/+; P{CaryP}attP2/+* ***yw>rpr* (attP2)**: *w*/ y^1 w^*; P{UAS-rpr.C}14/+; +/+*

For male animals the second X chromosome was Y.